Synthesis, Structure, Photoluminescence and Thermal Expansion of a Rare Earth Formate Oxalate Framework①

Hadi Abdul Nada[a, b] LI Wei[a]
FENG Guo-Qiang[c] LU Pei-Xiang[a②]
[a] (*School of Physics, Huazhong University of Science and Technology, Wuhan* 430074*, China*)
[b] (*Department of Physics, College of Education, University of Al-Qadisiya, Iraq*)
[c] (*Department of Physics and Mechanical & Electrical Engineering, Hubei University of Education, Wuhan* 430205*, China*)

ABSTRACT A new lanthanide formate oxalate framework **[**$Eu(C_2O_4)(HCOO)]_n$ (**1**) has been synthesized *via* hydrothermal method and characterized by single-crystal X-ray diffraction (SC-XRD). The framework crystallizes in the orthorhombic *Pnma* space group, with a = 7.0984(4), b = 6.6442(3), c = 10.6793(6) Å, V = 503.68(4) Å^3, Z = 3, C_3HO_6Eu, M_r = 285.00 g/mol, D_c = 3.7581 g/cm^3, $F(000)$ = 520.3796, μ = 12.413 mm^{-1}, the final R = 0.0264 and wR = 0.0628 for 797 observed reflections with $I > 2\sigma(I)$. The photoluminescence (PL) measurements reveal the significant red emission of the framework is dominated by the ($^5D_0 \rightarrow {}^7F_2$) electronic transition at 614 nm. Further variable-temperature powder X-ray diffraction (VT-PXRD) indicates that framework **1** shows slight negative thermal expansion (NTE) along the *a*-axis, and positive thermal expansion (PTE) along the *b* and *c* axes.

Keywords: formate oxalate framework, hydrothermal method, photoluminescence, thermal expansion; DOI: 10.14102/j.cnki.0254-5861.2011-1683

1 INTRODUCTION

Lanthanide-organic frameworks are emerging types of materials which have potential applications in the fields of optoelectronics like optical display panels and light-emitting diodes (LEDs) due to their outstanding optical properties[1]. These hybrid frameworks are composed by organic ligands and metal ions within a homogeneous structure establishing an extensive range of emissive phenomena, for instance linker-based luminescence[2], metal-based emission[3] or antenna effects[4]. Both inorganic and organic moieties can provide the platforms to produce luminescence, typically the origin of luminescence emission widely observed in lanthanide MOFs via the so-called (antenna effect) which is often referred to as the ligand-to-metal charge-transfer (LMCT), since the strongly absorbing ligand acts as a receiving antenna for the bond metal ion. In addition, cooperative functionalities of permanent porosity and luminescence property qualified luminescent MOFs as a very attractive new class of sensing materials[5, 6].

Trivalent lanthanide Ln(III) ions produce attractive optical properties. Recently, the luminance studies of rare earths metals that are synthesized with various organic ligands have been conducted. Ln(III) chelates provide narrow band emissions and very pure luminescence using UV-VIS excitation[7]. This

Received 20 April 2017; accepted 5 July 2017 (**CCDC 1553856**)
① This work was supported by the National Natural Science Foundation of China (21571072)
② Corresponding authors. Prof. Lu Pei-Xiang. E-mail: lupeixiang@hust.edu.cn; Dr. Feng Guo-Qiang. E-mail: gqfeng627@hust.edu.cn

sensitized luminescence of the lanthanide compounds is commonly used for optical materials, biological applications, electroluminescent devices, optical amplifier or laser and sensors[8, 9]. Luminescence of europium (Eu^{3+}) and terbium (Tb^{3+}) compounds takes the trending due to the narrow f-f transitions, especially the compounds of Eu^{3+} have attracted a lot of attention because of their good sensitization luminescence that can be carried out through the antenna effect as well as the line of emission spectra look mostly sharp as it depends on the crystal field around the metal ions. Furthermore a great attention has been paid to the luminescence of Eu^{3+} ions owing to the ability of acting as phosphors and progress of materials[10]. It is well-known that rare earth organic frameworks have attracted comprehensive interest over the past few years because not only their interesting applications but also their luminescence which originated from intra 4f or 4f–5d transitions[11]. This specific luminescence is characterized by high luminescence quantum yield, narrow bandwidth, long life time, large Stokes shifts, and ligand dependent luminescence sensitization[12, 13].

Herein we show crystalline framework materials incorporated both inorganic and organic moieties are attracting candidates because of their wide chemical and structural varieties that propose opportunities for making many technologically relevant properties[14]. Notably, the dense hybrid systems incorporated with infinite inorganic connectivity, like metal-oxygen-metal (M-O-M) arrays, can present the topological characteristics desired for certain types of physical properties[15]. In the present work, a new lanthanide-organic framework **[**$Eu(C_2O_4)(HCOO)]_n$ (**1**), constituted by three basic building blocks with inorganic M-O-M chains and two organic bridging ligands of oxalate $(C_2O_4)^{2-}$ and formate ($HCOO^-$) ions, has been successfully prepared by hydrothermal method, and the crystal structure has been described in details. The PL experiment shows that framework **1** exhibits strong red emission spectrum from the characteristic luminescence of Eu^{3+}. In addition, VT-PXRD experiment reveals that compound **1** displays NTE along the *a* axis, whereas *b* and c axes display PTE, which can be ascribed to the aforementioned structure arrangement.

2 EXPERIMENTAL

2. 1 Synthesis of $[Eu(C_2O_4)(HCOO)]_n$

All chemicals and solvents were of regent grade and used as received without further purification. We prepared the title compound in a Pyrex-lined steel bomb (autogenous pressure) at temperature around 200 °C over a week[16]. Crystals were obtained by heating an aqueous suspension of Eu oxalate hydrate $Eu_2(C_2O_4)_3{\cdot}10H_2O$ with 15 mmol of acid oxalic dihydrate in 10 mL of water for a week. By varying the heating time less or more than 7 days, it has been observed that no single crystals were developed. The final product was harvested by filtration, washed with water and ethanol, and then dried in air and the production rate was 53%.

2. 2 Structure determination

PXRD patterns for framework **1** were collected on a (Empyrean, PANalytical, 40 kV, 40 mA) diffractometer by using Cu$K\alpha$ (1.540598 Å) radiation. Single-crystal X-ray data of **1** were collected at room temperature using OXFORD Diffraction Rigaku. XtalABmin^{TM} Diffractometer. The elemental analysis (EA) was performed on an Elementar Vario Micro Cube ELIII elemental analyzer.

Single-crystal X-ray diffraction data were collected on an Oxford CCD diffractometer with graphite-monochromated Mo$K\alpha$ radiation (λ = 0.71073 Å). The structure was solved by direct methods and successive Fourier difference syntheses, and refined by full-matrix least-squares procedure on F^2 with anisotropic thermal parameters for all non-hydrogen atoms using programs SHELXS-97 and SHELXL-97, respectively[17]. Hydrogen atoms were located by geometric calculations and refined using a riding mode. X-Seed was used as an interface for the SHELX programs[18]. Data reduction and absorption corrections were applied and determined using the CrysAlis^{Pro} program[19]. A total of 3707 reflections

($3.61 \leqslant \theta \leqslant 32.93°$) were collected with 893 unique ones, of which 797 observed reflections with $I > 2\sigma(I)$ were observed and used for structural illustration. At convergence, the final $R = 0.0264$ and $wR = 0.0628$ ($w = 1/[\sigma^2(F_o^2) + (0.0506P)^2 + 0.9326P]$, where $P = (F_o^2 + 2F_c^2)/3$), goodness-of-fit = 1.0349, $(\Delta\rho)_{max} = 3.6774$ and $(\Delta\rho)_{min} = -1.6523$ e/Å^3. The selected bond lengths and bond angles are listed in Table 1.

Table 1. Selected Bond Lengths (Å) and Bond Angles (°)

Bond	Dist.	Bond	Dist.	Bond	Dist.
Eu(1)–O(1)	2.464(4)	Eu(1)–O(1)$^{\#3}$	2.490(3)	Eu(1)–O(3)	2.492(4)
Eu(1)–O(1)$^{\#1}$	2.490(3)	Eu(1)–O(2)	2.436(3)	Eu(1)–O(3)$^{\#1}$	2.442(4)
Eu(1)–O(1)$^{\#2}$	2.464(4)	Eu(1)–O(2)$^{\#2}$	2.436(3)	Eu(1)–O(4)	2.472(5)
Angle	(°)	Angle	(°)	Angle	(°)
O(1)–Eu(1)–O(1)$^{\#1}$	140.8(1)	O(1)$^{\#2}$Eu(1)–O(2)$^{\#2}$	126.1(1)	O(2)–Eu(1)–O(4)	70.4(9)
O(1)–Eu(1)–O(1)$^{\#2}$	66.5(1)	O(1)$^{\#2}$–Eu(1)–O(3)	64.4(7)	O(2)$^{\#2}$–Eu(1)–O(3)	114.3(9)
O(1)–Eu(1)–O(1)$^{\#3}$	100.3(1)	O(1) $^{\#2}$–Eu(1)–O(4)	70.7(6)	O(2)$^{\#2}$–Eu(1)–O(4)	70.4(9)
O(1)–Eu(1)–O(2)	126.1(1)	O(1)$^{\#3}$Eu(1)–O(2)	132.8(1)	O(3)$^{\#1}$–Eu(1)–O(1)	64.7(8)
O(1)–Eu(1)–O(2) $^{\#2}$	66.3(1)	O(1)$^{\#3}$–Eu(1)–O(2)	72.4(1)	O(3)$^{\#1}$–Eu(1)–O(2)	78.5(8)
O(1)–Eu(1)–O(3)	64.4(6)	O(1)$^{\#3}$–Eu(1)–O(3)	76.5(6)	O(3)–Eu(1)–O(4)	125.6(1)
O(1)–Eu(1)–O(4)	70.7(6)	O(1)$^{\#3}$–Eu(1)–O(4)	142.2(7)	O(4)–Eu(1)–O(2)$^{\#2}$	70.4(9)
O(1)$^{\#2}$–Eu(1)–O(1)	140.8(1)	O(2)–Eu(1)–O(2)$^{\#2}$	129.3(1)		
O(1)$^{\#2}$–Eu(1)–O(2)	66.3(1)	O(2)–Eu(1)–O(3)	114.3(1)		

Symmetry codes: #1: 0.5+*x*, 0.5–*y*, 0.5–*z*; #2: *x*, *y*, 0.5–*z*; #3: 0.5+*x*, 0.5–*y*, *z*

2. 3 Variable temperature powder X-ray diffraction

VT-PXRD experiments were performed on a Bruker a D8-discover X-ray diffractometer, where Cu$K\alpha$ radiation ($K\alpha_1 = 1.5406$ and $K\alpha_2 = 1.5443$ Å) at 40 kV, 30 mA, 2 mm divergence slit; 0.6 mm anti-scatter slit; 0.2 mm receiving slit; monochromatic; 0.1 mm detector slit. The temperature was adjusted by a cryostat with temperature-adjusting error less than 1 K. The angular scanning range was 10～50º with the step of 0.01º and scanning rate of 1*s*/step. The cell parameters of variable temperatures were refined by Rietveld method using GSAS software. The in-situ VT-PXRD patterns were collected over the range of 180～280 K, with a 20 K interval.

3 RESULTS AND DISCUSSION

3. 1 Structure description

The single-crystal X-ray diffraction study revealed that the framework of **1** has asymmetric units, as illustrated in Fig. 1. The structure of compound **1** is a 3-D hybrid framework in orthorhombic *Pnma* space group. The dimensionalities of its inorganic and organic connectivity are 1-D and 2-D, respectively. The 1-D inorganic chains contain 9-coordinated europium polyhedra (EuO_9) and their faces participate in forming infinite zigzag chains along the [100] direction. To form the 2-D organic connectivity, europium chains are bridged by formate ligands along the [010] direction to generate infinite 2-D layers, and the layers nearby are subsequently bridged by the oxalate ligands along the [001] direction to make a 3-D framework structure.

Finally, the structure for **1** is built up from Eu atoms sharing all their oxygen atoms with oxalate and formate ligands, thus giving rise to a 3D framework structure (Fig. 1). The bond distances of Eu(1)–O(4) and O(1)–C(2) are 2.472(5) and 1.274(6) Å, respectively, and the bond angles are as follows: O(4)$^{\#5}$–C(3)–O(3) 125.5(6) and O(1)–C(2)–O(2)$^{\#6}$ 126.1(8)°. For comparison, in the isostructural compound $Ce(C_2O_4)(HCOO)$ previously reported[16], Ce–O(4) = 2.503(3), O(1)–C(1) = 1.237(8) Å and O(1)–C(1)–O(2) = 127.3(6), O(4)–C(2)–O(3) = 125.7(4)°.

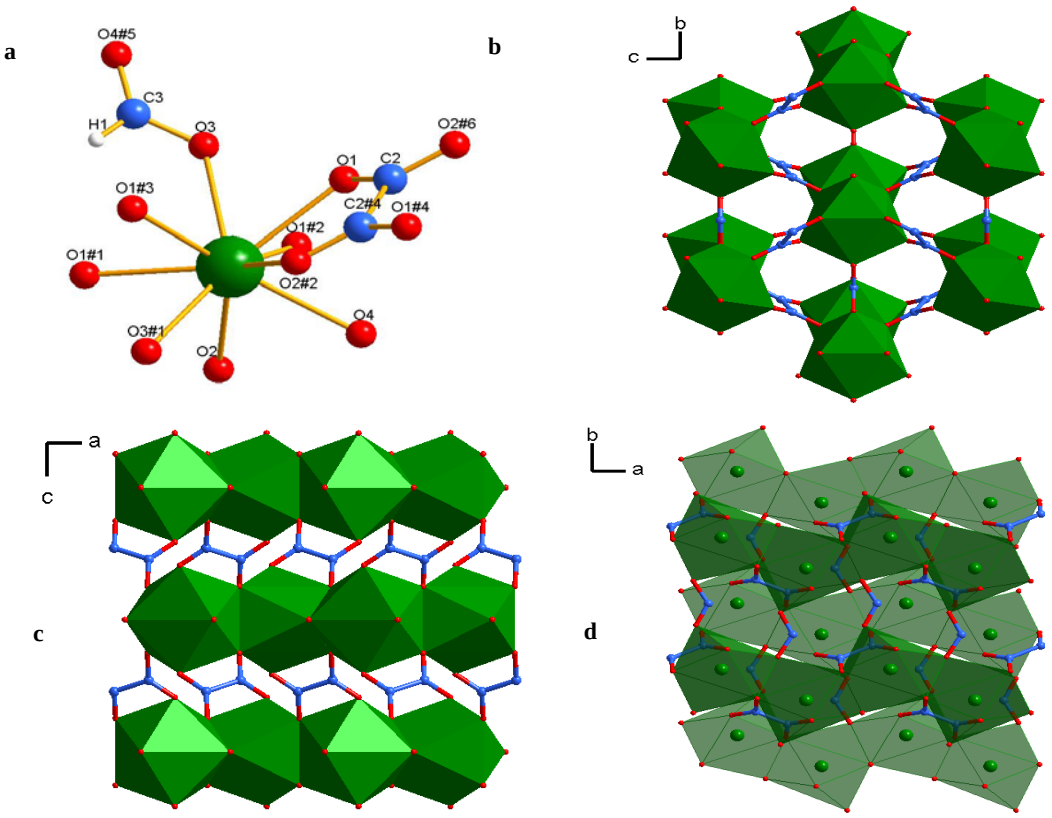

Fig. 1. Illustration of 1 with asymmetric unit (a); Framework structure of 1 normal to the (b) {100}, (c) {010} and (d) {001} planes, respectively; Color scheme: Eu, green; O, red; C, blue; hydrogen atoms have been deleted for clarity in (b～d). Symmetry codes: #4: –*x*, –*y*, –*z*, #5: *x*, 1+*y*, *z*, #6: –*x*, –*y*, –0.5+*z*

3. 2 Photoluminescent property

The PXRD patterns shown in Fig. 2 confirm the purity of the as-synthesized compound **1**. Then PL measurements were performed using pulsed laser He-Cd (325 nm) (horiba Jobin Yvon) on the pure sample at room temperature. Fig. 3 shows the normalized PL measurement spectra of **1** with an excitation wavelength of the pulsed ultraviolet He-Cd laser 325 nm at room temperature. Notably, **1** shows emission region 300 ～ 800 nm and the characteristic peak of Eu^{3+} transition is observed. The resonance energy levels of europium ions along with various luminescence transitions are presented in Table 2[20, 21]. The PL emission of the Eu^{3+} ions indicates emission lines in the visible region with a comparatively simple energy level structure.

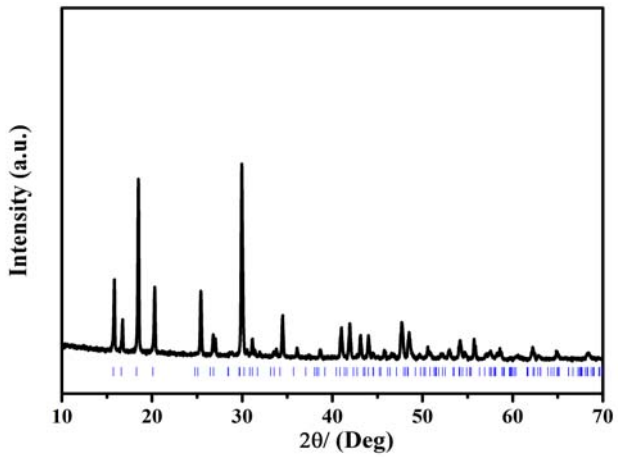

Fig. 2. PXRD pattern of the as-synthesized $[Eu(C_2O_4)(HCOO)]_n$. The black line is the experimental pattern and the blue vertical markers indicate the allowed Bragg reflection

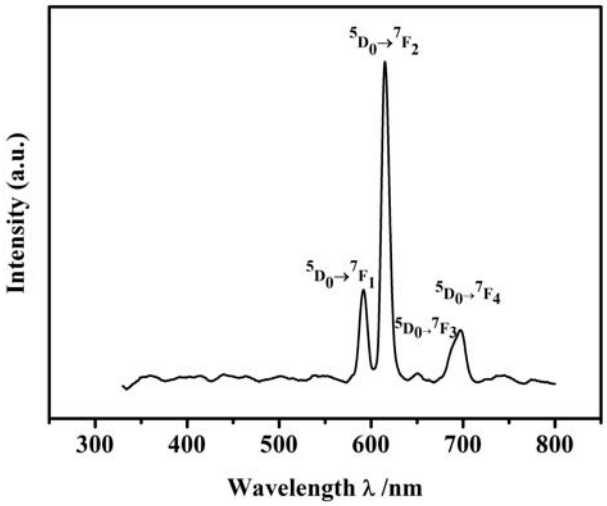

Fig. 3. PL spectrum from 1

Table 2. Energy Levels and Luminescent Transition for Europium

Upper energy levels (energy cm^{-1})	Lower levels	λ (nm)
Eu^{+3} $^5D_3$(24500)	-	-
$^5D_2$(21500)	-	-
$^5D_1$(19020)	$^7F_1$,$^7F_2$,$^7F_3$,$^7F_5$,$^7F_6$	538, 554, 583, 655, 701
$^5D_0$(17260)	$^7F_0$,$^7F_1$,$^7F_2$,$^7F_3$,$^7F_4$	580, 596, 614, 651, 694

Herein, the luminescence for Eu^{3+} ions may rise from the $^5D_0 \rightarrow {}^7F_J$ transition, where (J = 0, 1, 2, 3, 4) levels are dependent on the triplet state energy of the donor, thus the energy is fundamentally transferred to $^5D_0$ corresponding to 17260 cm^{-1}[7, 20]. As shown in Fig. 3, **1** exhibits four sets of characteristic emission bands from Eu^{3+} ions in the visible spectral region with different intensities. The emission peak is centered at 590 nm originating from the $^5D_0 \rightarrow {}^7F_1$ transition. The most prominent emission is located at 614 nm and is dominated by electric dipole transition of Eu^{3+}, which corresponds to the strong red luminescence emission output. In fact, the $^5D_0 \rightarrow {}^7F_2$ transition of Eu^{3+} ion originates from electric dipole (ED) and is sensitive to the coordination environment around the Eu^{3+} ion, it denotes that the Eu^{3+} ion possesses non-centrosymmetric environment that agrees with the resulting single crystal diffraction pattern. The PL peaks at 651 and 696 nm can be assigned to $^5D_0 \rightarrow {}^7F_3$, and $^5D_0 \rightarrow {}^7F_4$, respectively. In contrast, the emission intensity from $^5D_0 \rightarrow {}^7F_1$ transition depends on the crystal field dominated by magnetic dipole (MD), which is insensitive to the site symmetry, as shown in the emission spectrum in Fig. 3. And the intensity of the $^5D_0 \rightarrow {}^7F_2$ transition is about 3 times stronger than that of the $^5D_0 \rightarrow {}^7F_1$ transition, which indicates that there is no inversion center at the Eu^{3+} sites.

3. 3 Thermal expansion study

Thermal expansion behaviour of framework **1** was studied *via* variable-temperature X-ray diffraction (VT-XRD) experiments. Fig. 4(a) shows the measured temperature-dependent variations in the lattice parameters between 180 and 280 K with a 20 K interval. It's obvious that axes *b* and *c* show positive thermal expansion (PTE) about +0.07% and +0.09%, respectively, whereas *a* axis exhibits negative thermal expansion (NTE) about −0.03%. The obtained average coefficients of thermal expansion along three orthogonal axes and the volumetric thermal expansion coefficients are a_a = –2.0(5), a_b = 8.2(14), a_c = 7.6(11) and a_V = 16.7(25) MK^{-1}, respectively, *via* linear fits using the PASCal software[22]. Furthermoer, Fig. 4(b) presents different direction thermal expan-

sions of **1** based on the PASCal program calculation. Notably, the NTE magnitude of **1** is slightly smaller than the dense rare earth formate framework $[NH_2CHNH_2][Er(HCOO)4]$ (α_b = −7.1(3) MK^{-1})[23], the most well-known NTE material cubic zirconium tungstate, ZrW_2O_8 (α = −9 MK^{-1})[24] and rigid MOF-5 (α = −9 MK^{-1})[25], but significantly lower than other protypical NTE MOFs, such as flexible silver(I) 2-methylimidazolate (α_c = −24.5 MK^{-1})[26], $[Zn_2(fu\text{-}L)_2dabco]$[27] and $InD(BDC)_2$ (BDC = 1,4-benzenedicarboxylate, α_c= −3.5 MK^{-1})[28].

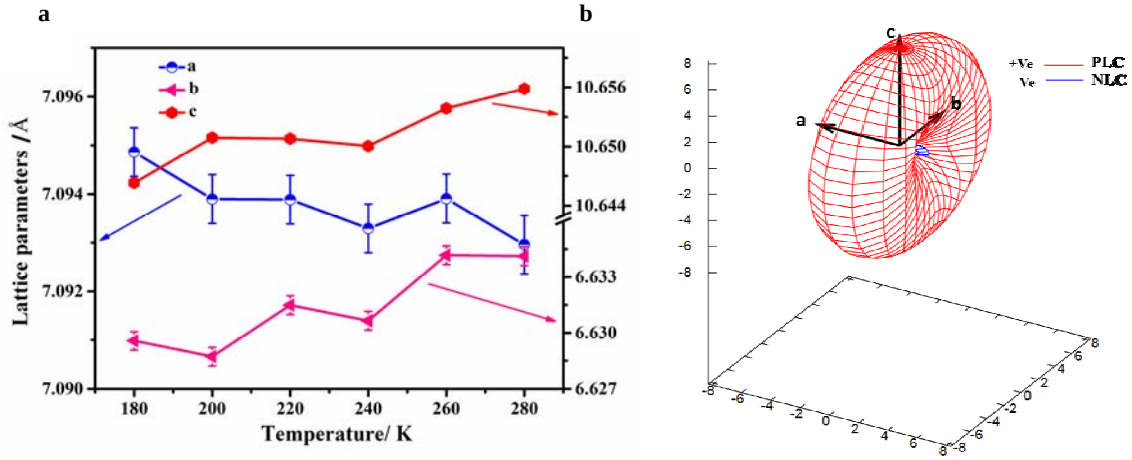

Fig. 4. (a) Evolution of lattice parameters *a*, *b* and *c* of 1 dependent on temperature (the solid lines there are to guide the eye); (b) Different direction thermal expansions of 1 based on the PASCal program calculation. Note: the positive and negative thermal expansions are illustrated in red and blue grids, respectively

Overall, the NTE along *a* axis could be explained by the following reasons. First of all, with the temperatue increase, the bond lengths of formate and oxalate ligands expand along the [010] and [001] directions, respectively (see Fig. 4(b)). Such variations are more likely to induce the flexing of EuO_9 polyhedra. However, as stated previously, these EuO_9 polyhedras share their faces to construct 1-D infinite zigzag chains along the [100] direction (see Fig. 4(a), (b)). The flexing and the stronger interaction of the polyhedral chains maybe restrict the expanding along [100], thus giving rise to NTE along the [100] direction.

In this work, a 3-D hybrid framework **1** was successfully prepared through hydrothermal method and characterized by SC-PXRD. The photoluminescence experiment shows that **1** gave a high luminescence at 614 nm, which originated from the $^5D_0 \rightarrow {}^7F_2$ transition of Eu^{3+} ion, implying red emission output of **1**. Furthermore, VT-PXRD study revealed that **1** shows a slight NTE along the *a*-axis and PTE along the *b*- and *c*- axes, which indicates this material's anisotropic nature in response to the temperature variation. To conclude, **1** could have potential applications in solid state lighting and field emission displays. emission displays.

4 CONCLUSION

REFERENCES

(1) (a) Zhang, H. J.; Wang, X. Z.; Zhu, D. R.; Song, Y.; Xu, Y.; Xu, H.; Shen, X.; Gao, T.; Huang, M. X. Novel 3D lanthanide-organic frameworks with an unusual infinite nanosized ribbon $[Ln_3(\mu_3\text{-}OH)_2(\text{-}CO_2)_6]^+_n$ (Ln ¼ Eu, Gd, Dy): syntheses, structures, luminescence, and magnetic properties. *Cryst Eng.Comm.* **2011**, 13, 2586−2592. (b) Feng, X.; Liu, B.; Wang, L. Y.; Zhao, J. S.; Wang, J. G.; Wang, N. S.; Shi, X. G. A series of lanthanide-organic polymers incorporating nitrogen-heterocyclic and aliphatic carboxylate mixed-ligands: structures, luminescent and magnetic properties. *Dalton Trans*. **2010**, 39, 8038−8049. (c) Dai, F.; Cui, P.; Ye, F.; Sun, D. An open neodymium-organic framework with the NbO structure type based on binuclear SBU involved in situ generated format. *Cryst. Growth Des*. **2010**, 10, 1474−1477. (d) Zhu, W. H.; Wang, Z. M.; Gao, S. Two 3D

porous lanthanide-fumarate-oxalate frameworks exhibiting framework dynamics and luminescent change upon reversible de-and rehydration. *Inorg. Chem*. **2007**, 46, 1337−1342.

(2) (a) Du, M.; Jiang, X. J.; Zhao, X. J. Molecular tectonics of mixed-ligand metal-organic frameworks: positional isomeric effect, metal-directed assembly, and structural diversification. *Inorg. Chem*. **2007**, 46, 3984−3985; (b) Lan, A. J.; Han, L.; Yuan, D. Q.; Jiang, F. L.; Hong, M. C. A blue luminescent inorganic-organic hybrid with infinite $[Cd_3(l3\text{-}OH)_2(l2\text{-}Cl)_2]$ connectivity. *Inorg. Chem. Commun*. **2007**, 10, 993−996; (c) Wang, X. L.; Bi, Y. F.; Lin, H. Y.; Liu, G. C. Three novel Cd(III) metal-organic frameworks constructed from mixed ligand of dipyrido [3,2-d:2,3-f] quinoxalin and benzene-dicarboxylate: from a 1-d ribbon, 2-d layered network, to a 3-D artichitecture. *Cryst. Growth Des*. **2007**, 7, 1086−1091.

(3) (a) Sonnauer, A.; Nather, C.; Hoppe, H. A.; Senker, J.; Stock, N. Systematic investigation of lanthanide phosphonate thanesulfonate framework structure by high-throught methods, $Ln(O_3P\text{-}C_2H_4\text{-}SO_3)(H_2O)$ (Ln = La-Dy). *Inorg. Chem*. **2007**, 46, 9968−9974; (b) Gandara, F.; Garcia-Cortes, A.; Cascales, C.; Gomez-Lor, B.; Gutierrez-Puebla, E.; Iglesias, M.; Monge, A.; Snejko, N. Rare earth arenedisulfonate metal-organic frameworks: an approach toward polyhedral diversity and variety of functional compound. *Inorg. Chem*. **2007**, 46, 3475−3484.

(4) (a) de Lill, D. T.; de Bettencourt-Dias, A.; Cahill, C. L. Exploring lanthanide luminescence in metal-organic frameworks: synthesis, structure, and guest-sensitized luminescence of a mixed europium/teribium-adipate framework and a terbium-adipate framework. *Inorg. Chem*. **2007**, 46, 3960−3965; (b) McManus, G. J.; Perry, J. J.; Perry, M.; Wagner, B. D.; Zaworotko, M. J. Exciplex fluorescence as a diagnostic probe of structure in coordination polymers of Zn^2 and 4,4-bipyridine containing interacted pyrene and enclathrated aromatic solvent guests. *J. Am. Chem. Soc*. **2007**, 129, 9094−9101; (c) Chen, B. L.; Yang, Y.; Zapata, F.; Qian, G. D.; Luo, Y. S.; Zhang, J. H.; Lobkovsky, E. B. Enhanced near-infrared-luminescence in an erbium tetrafluoroterephthalate framework. *Inorg. Chem*. **2006**, 45, 8882−8886.

(5) Hatanaka, M.; Hirai, Y.; Kitagawa, Y.; Nakanishi, T.; Hasegawa, Y.; Morokuma, K. Organic linkers control the thermosensitivity of the emission intensities from Tb(III) and Eu(III) in a chameleon polymer. *Chem. Sci.* **2017**, 8, 423−429.

(6) Rossin, A.; Giambastiani, G.; Peruzzini, M.; Sessoli, R. Amine-templated polymeric lanthanide formates: synthesis, characterization, and applications in luminescence and magnetism. *Inorg. Chem*. **2012**, 51, 6962−6968.

(7) Latva, M.; Takalo, H.; Mukkala, V. M.; Matachescu, C.; Rodriguez-Ubis, J. C.; Kankare, J. Correlation between the lowest triplet state energy level of the ligand and lanthanide(III) luminescence quantum yield. *J. Lumin.* **1997**, 75, 149−169.

(8) Bunzil, J. C. G.; Piguet, C. Taking advantage of luminescent lanthanide ions. *Chem. Soc. Rev*. **2005**, 34, 1048−1077.

(9) Cui, Y. G.; Chen, L. B.; Qian, D. G. Lanthanide metal-organic frameworks for luminescent sensing and light-emitting applications. *Coord. Chem . Rev*. **2014**, 273, 76−86.

(10) Vicentini, G.; Zinner, B. L.; Zukerman-Schpector, J.; Zinner, K. Luminescence and structure of europium compounds. *Coord. Chem. Rev.* **2000**, 196,353−382.

(11) (a) Robin, Y. A.; Fromm, M. K. Coordination polymer networks with O- and N-donors: what they are, why and how they are made. *Coord. Chem. Rev.* **2006**, 250, 2127-2157; (b) Chandler, D. B.; Cramb, T. D.; Shimizu, H. K. G. Microporous metal-organic frameworks in a stepwise manner from luminescence building blocks. *J. Am. Chem. Soc.* **2006**, 128, 10403−10412.

(12) Shang, M.; Geng, D.; Kang, X; Yang, D.; Zhang, Y.; Lin, J. Hydrothermal derived $LaOF:Ln^{3+}$ (Ln = Eu, Tb, Sm, Dy, Tm, and/or Ho) nanocrystals with multicolor-tunable emission properties. *Inorg. Chem*. **2012**, 51, 11106−11116.

(13) Sun, X.; Zhang, W. Y.; Du, P. Y.; Yan, G. Z.; You, P. L.; Yan, H. C. From trifluoroacetate complex precursors to monodisperse rare-earth fluoride and oxyfluoride nanocrystals with diverse shapes through controlled fluorination in solution phase. *Chem.-Eur. J*. **2007**, 13, 2320−2332.

(14) (a) Cheetham, A. K.; Rao, C. N. R.; Feller, R. K. Structural diversity and chemical trends in hybrid inorganic-organic framework materials. *Chem. Commun.* **2006**, 4780–4795. (b) Rao, C. N. R.; Cheetham, A. K.; Thirumurugan, A. Hybrid inorganic-organic materials: a new family in condensed matter physics. *J. Phys. Condens. Matter.* **2008**, 20, 083202. (c) Kurmoo, M. Magnetic metal-organic frameworks. *Chem. Soc. Rev.* **2009**, 38, 1353–1379.

(15) Rao, C. N. R.; Natarajan, S.; Vaidhyanathan, R. Metal carboxylates with open architectures. *Angew. Chem. Int. Ed.* **2004**, 43, 1466–1496.

(16) Romero, S.; Mosset, A.; Trombe, J. C. Two new families of lanthanide mixed-ligand complexes, oxalate-carbonate and oxalate-formate: synthesis and structure of $[Ce(H_2O)]_2(C_2O_4)_2(CO_3)\cdot 2.5\ H_2O$ and $Ce(C_2O_4)(HCO_2)$. *J. Solid State Chem.* **1996**, 127, 256–266.

(17) Sheldrick, G. M. A short history of SHLX. *Acta Crystallogr. Sect. A* **2008**, 64, 112–122.

(18) Barbour, L. J. X-seed – a software tool for supermolecular crystallography. *J. Supramol. Chem*. **2001**, 1, 189–191.

(19) *CrysAlis*^{Pro}, Oxford Diffraction Ltd., Version 1.171.34.34.

(20) Freeman, J. J.; Crosby, A. G. Spectra and decay times of the luminescence observed from chelated rare earth. *J. Phys. Chem*. **1963**, 67, 2717.

(21) Georges, J.; Mermet, M. J. Simultaneous time-resolved florescence and thermal lens measurements: application to energy transfer studies in europium chelates. *Spectroscopic. Acta* part A **1993**, 49, 397–404.

(22) Cliffe, M.; Goodwin, A. L. PASCal: a principle axis strain calculator for thermal expansion and compressibility determination. *J. Appl. Cryst*. **2012**, 45, 1321–1329.

(23) Zhang, Z.; Jiang, X.; Feng, G.; Lin, Z.; Hu, B.; Li, W. Mechanical properties and negative thermal of a dense rare earth formate framework *Journal of Slid State Chemistry* **201**6, 233, 289–293.

(24) Mary, A.; Evans, J. S. O.; Vogt, T.; Sleight, A. W. Negative thermal expansion from 0.3 to 1050 kelvin in Zrw_2O_5. *Science* **1996**, 272, 90–92.

(25) Lock, N.; Wu, Y.; Christensen, M.; Cameron, L. J.; Peterson, V. K.; Bridgeman, A. J.; Kepert, C. J.; Iverson, B. B. Elucidating negative thermal expansion in MOF-5. *J. Phys. Chem. C* **2010**, 114, 16181–16186.

(26) Ogborn, J. M.; Collings, I.; Moggach, S. A.; Thompson, A. L.; Goodwin, A. L. Supermolecular mechanics in a metal-organic framework. *Chem. Sci*.**2012**, 3, 3011–3017.

(27) Henk, S.; Schneemann, A.; Fischer, R. A. Massive anisotropic thermal expansion and thermo-responsive breathing in metal-organic frameworks modulated by linker functionalization. *Adv. Funt. Mter*. **2013**, 23, 5990–59996.

(28) Collings, I. E.; TucKer, M. G.; Keen, D. A.; Goodwin, A. L. Geometric switching of linear to area negative thermal expansion in uniaxial metal-organic frameworks. *CrystEngComm*. **2014**, 16, 3498–3506.